Journal of Orthopaedic Translation 39 (2023) 124–134

Contents lists available at ScienceDirect

Journal of Orthopaedic Translation

journal homepage: www.journals.elsevier.com/journal-of-orthopaedic-translation

Original Article

Cerebrospinal fluid-derived extracellular vesicles after spinal cord injury promote vascular regeneration via PI3K/AKT signaling pathway

Chengjun Li [a,b,c], Tian Qin [a,b,c], Yuxin Jin [a,b,c,***], Jianzhong Hu [a,b,c], Feifei Yuan [a,b,c], Yong Cao [a,b,c,**], Chunyue Duan [a,b,c,*]

[a] Department of Spine Surgery and Orthopaedics, Xiangya Hospital, Central South University, Xiangya Road 87, Changsha, 410008, China
[b] Key Laboratory of Organ Injury, Aging and Regenerative Medicine of Hunan Province, Xiangya Road 87, Changsha, 410008, China
[c] National Clinical Research Center for Geriatric Disorders, Xiangya Hospital, Central South University, Xiangya Road 87, Changsha, 410008, China

ARTICLE INFO

Keywords:
Spinal cord injury
Cerebrospinal fluid
Extracellular vesicles
Vascular regeneration
PI3K-AKT pathway

ABSTRACT

Background: The cerebrospinal fluid (CSF), which surrounds the brain and spinal cord, is predominantly produced by the choroid plexus of the ventricle. Although CSF-derived extracellular vesicles (CSF-EVs) may be utilized as diagnostic and prognostic indicators for illnesses of the central nervous system (CNS), it is uncertain if CSF-EVs may have an impact on neurological function after spinal cord injury (SCI).

Methods: Here, we isolated EVs using ultracentrifugation after extracting CSF from Bama miniature pigs. We then combined CSF-EVs with hydrogel and put it on the spinal cord's surface. To determine if CSF-EVs had an impact on mice's neurofunctional recovery, behavioral evaluations were employed. Both in vitro and in vivo, the effect of CSF-EVs on angiogenesis was assessed. We investigated whether CSF-EVs stimulated the PI3K/AKT pathway to alter angiogenesis using the PI3K inhibitor LY294002.

Results: CSF-EVs were successfully isolated and identified by transmission electron microscope (TEM), nano-tracking analysis (NTA), and western blot. CSF-EVs could be ingested by vascular endothelial cells as proved by in vivo imaging and immunofluorescence. We demonstrated that CSF-EVs derived from pigs with SCI (SCI-EVs) showed a better effect on promoting vascular regeneration as compared to CSF-EVs isolated from pigs receiving laminectomy (Sham-EVs). Behavioral assessments demonstrated that SCI-EVs could dramatically enhance motor and sensory function in mice with SCI. Western blot analysis suggested that SCI-EVs promote angiogenesis by activating PI3K/AKT signaling pathway, and the pro-angiogenetic effect of SCI-EVs was attenuated by the application of the LY294002 (PI3K inhibitor).

Conclusion: Our study revealed that CSF-EVs could enhance vascular regeneration by activating the PI3K/AKT pathway, hence improving motor function recovery after SCI, which may offer potential novel therapeutic options for acute SCI.

The translational potential of this article: This study demonstrated the promotion of vascular regeneration and neurological function of CSF-derived exosomes, which may provide a potential therapeutic approach for the treatment of spinal cord injury.

1. Introduction

Spinal cord injury (SCI) usually causes motor, sensory and autonomic dysfunction, and there is currently no curative treatment [1,2]. The limited regenerative capacity of microvasculature is one of the factors contributing to the difficulty of restoring neurological function after SCI [3]. Primary SCI frequently disrupts the blood-spinal cord barrier (BSCB) and vascular network, and in addition, the local inhibitory environment brought on by secondary SCI also hinders angiogenesis [4]. An intact vascular network can provide adequate nutrition for spinal cord tissue repair and provide a functional scaffold for axonal regeneration [3]. Therefore, it is crucial to find an effective way of promoting angiogenesis after SCI.

Cerebrospinal fluid (CSF) is produced by the choroid plexus, which

* Corresponding author. Department of Spine Surgery and Orthopaedics, Xiangya Hospital, Central South University, Xiangya Road 87, Changsha, 410008, China.
** Corresponding author. Department of Spine Surgery and Orthopaedics, Xiangya Hospital, Central South University, Xiangya Road 87, Changsha, 410008, China.
*** Corresponding author. Department of Spine Surgery and Orthopaedics, Xiangya Hospital, Central South University, Xiangya Road 87, Changsha, 410008, China.
E-mail addresses: 645391176@qq.com (Y. Jin), caoyong1912@163.com, xycaoyong@csu.edu.cn (Y. Cao), docdcy@qq.com (C. Duan).

https://doi.org/10.1016/j.jot.2023.02.001
Received 19 September 2022; Received in revised form 2 February 2023; Accepted 6 February 2023

surrounds and supports the brain and spinal cord in the subarachnoid space and ventricles [5]. Numerous studies have shown that the molecular composition of CSF is closely related to the diagnosis and prognosis of central nervous system (CNS). Synaptosomal-associated protein 25 (SNAP-25) levels in CSF were decreased in Alzheimer's disease, which reflected synaptic dysfunction and degeneration [6,7]. Changes in CSF metabolites can predict the progression of autoimmune diseases of the CNS, such as multiple sclerosis [8]. SCI also affects the expression of the CSF protein profile [9]. Kwon BK et al. showed that ubiquitin C-terminal hydrolase L1 (UCH-L1) levels in cerebrospinal fluid, but not in serum, could predict the prognostic severity of SCI [10]. According to another study, some CSF microRNAs are associated with the degree of damage after SCI [11]. However, whether cerebrospinal fluid can be used in the treatment of SCI requires further research.

Extracellular vesicles (EVs) are membranous vesicles secreted by multiple cells, mainly for intercellular communication. According to the diameters, EVs were divided into exosomes (30 nm–150 nm) and ectosomes (50 nm–1 μm) [12,13]. It has been suggested that certain EV subtypes may impact the onset of CNS disorders by stimulating angiogenesis. After brain ischemia, EVs extracted from mesenchymal stromal cells (MSC) under hypoxic circumstances may encourage angiogenesis and enhance neurological recovery [14]. It has also been reported that other EVs derived from microglia, macrophages, or human urinary stem cells promote angiogenesis or enhance endothelial cell survival after SCI [15–17]. EVs are abundant in body fluids, and cerebrospinal fluid also contains a large amount of EVs [18–20]. MiR-126–5p, miR-99–5p, and miR-501–3p are expressed at elevated levels in CSF-EV of Parkinson's disease patients [21]. The altered microRNA profile may lead to more specialized diagnostic approaches. Another study found that CSF-EV may enhance neuronal survival ERK signaling in vitro [22]. However, whether CSF-derived extracellular vesicles (CSF-EVs) could promote angiogenesis and facilitate neurological function needs further investigation.

In the current study, we isolated CSF-EVs from pigs with SCI or laminectomy without SCI and demonstrated that SCI-EVs could promote vascular regeneration and improve neurological function after SCI through PI3K/AKT pathway. Our study may provide potential novel therapeutic approaches for the management of SCI.

2. Materials and methods

2.1. Animals and ethics

Female Bama miniature pigs (8 weeks old) weighing 10–13 kg were purchased from Aofei Biotechnology Co., Ltd, Hubei, China. Female C57BL/6 mice (8 weeks old) weighing 20–25 g were purchased from SJA Laboratory Animal Co., Ltd, Hunan, China. All animals were housed in the laboratory animal department at Central South University in Changsha, China, and were given free access to food and water. All the procedures were approved by Central South University's animal ethics committee.

2.2. SCI model of pigs and CSF-derived EVs characterization

Animals fasted 12 h before surgery. Telazol (5 mg/kg) and Xylazine (1 mg/kg) were intramuscularly injected to induce anesthesia, and propofol (8 mg/kg/h) was used to maintain the process. After routine disinfection with povidone iodine, a 13 cm incision was made in the middle of the back. To reveal the vertebrae, the fascia and muscles were obliquely dissected. Dorsal laminectomy was conducted at the T10 segment. A 50 g weight was dropped from a height of 20 cm to the medium surface of the spinal cord, and then a subsequent 100 g weight was added to compress the spinal cord for 5 min to ensure the successful establishment of the pigs' SCI model. After hemostasis with a gelatin sponge and wound cleaning with normal saline, the muscles and skin were sutured layer by layer. Laminectomy without injury was performed on pigs in the sham group. Penicillin was used intramuscularly for the first 3 days after surgery to prevent infection. CSF was collected 7 days after injury using a lumbar puncture. Briefly, after anesthetization, the pigs were fixed in the lateral decubitus position. A $16^{\#}$ (1.6*80 mm) lumbar puncture needle was used to vertically pierce the midpoint of the two iliac. When there is no resistance suddenly, it means that the needle has entered the spinal canal. Then, withdraw the needle core and collect 6–8 ml of CSF. After the CSF was collected from the injured spinal cord or sham groups pigs and then centrifuged at 300 g, 2000 g, and 10000 g to remove cells and cellular debris, the finally obtained supernatant was centrifuged at 100,000 g for 70 min to obtain purified EVs.

For transmission electron microscopy (TEM) detection, after the EVs were fixed with glutaraldehyde, the solution was added dropwise to the copper mesh, which was then treated with 2% phosphotungstic acid for 2 min at room temperature. The EVs were examined by TEM (FEI, United States). Nano-tracking analysis (NTA) was performed to detect the particle diameter range of EVs. We also performed western blot to analyze the surface markers of CD9, CD81, and Tsg101 of the EVs.

2.3. Characteristics of hydrogel

The components of light-cured hydrogel include 5% methacrylated gelatin (GelMA), 1.25% N-(2-aminothyl)-4-(4-(hydroxymethyl)-2-methoxy-5-nitrosophe-noxy) butanamide (NB) linked to the glycosaminoglycan hyaluronic acid (HA-NB) and 0.1% of the polymerization initiator lithium phenyl-2.4.6-trimethyl-benzoyl phosphinate (LAP), which were synthesized as previously described [23]. Scanning electron microscope (TEM, FEI, United States) was used to observe the micromorphology of the hydrogel. For in vitro degradation properties, the hydrogels were incubated at 37-degree balanced salt solution (HBSS) for 7, 14, 21, and 28 days. After freeze-drying, the hydrogel was weighed before (Wo) and after (Wt) incubation., respectively. The degradation rate was represented by calculating (Wo-Wt)/Wo.

2.4. SCI model of mice and in vivo imaging for EVs tracing

A modified Allen's method was used to establish the SCI model of mice. Mice were anesthetized with 0.3% sodium pentobarbital (75 mg/kg) intraperitoneally. A dorsal medium incision was made at the T10 level and muscles were separated. The spinal cord was exposed by removing the T10 segment lamina. A 10 g impactor fell freely from a height of 2 cm to the medium surface of the spinal cord. Laminectomy only without contusion was applied to the mice in the sham group. CSF-EVs (200 μg sham-CSF or SCI-EVs) were mixed with 4ul light-cured hydrogel. The injured spinal cord was covered with mixed hydrogel, which was then exposed to ultraviolet light for 5–9s. The hydrogel without CSF-EVs was administered to the mice in the control group. Muscles and skin were sutured in order, and penicillin was given to prevent infection. In the first week after surgery, the bladders of mice were manually squeezed twice a day to aid urination.

DiR is a lipophilic dye that labels cell membranes. For in vivo imaging, 200 μg sham-EVs or SCI-EVs (labeled by DiR, Yeasen, China) mixed with 4 μl hydrogel were placed on the surface of the injured spinal cord. The hydrogel mixture was exposed to ultraviolet light for 5–9s until the solidification of the hydrogel. At 7, 14, and 28 days after injury respectively, a Xenogen IVIS Imaging System (Caliper Life Sciences) was utilized to track the distribution and intensity of DiR-EVs in the injured area of the spinal cord.

2.5. EVs labeling and tracking

PKH26 kit (Sigma, United States) was used to label EVs. For in vitro EVs uptaking experiments of bEnd.3 cells, CSF-EVs were labeled with PKH26 following the manufacturer's instructions. A 24-well plate was seeded with 50,000 cells for each well. After adherence, 10 μg PKH26-labeled EVs were added to each well. The uptake of EVs by bEnd.3

cells were observed through immunofluorescence. 200 ug of PKH26-labeled EVs were combined with hydrogel and applied to the damaged spinal cord surface for in vivo tracking. The spinal cord specimens were harvested 7 days after injury for fixation, dehydration, and immunofluorescence staining.

2.6. Behavioral assessment

BMS scores were employed to assess locomotor ability as previously described [24]. The BMS scores ranged from 0 (completely paralyzed) to 9 (normal locomotion). Two skilled observers who were not informed of the experiment grouping assessed the locomotor capacity independently, and the final score was calculated by averaging. Before the injury and 1, 3, 7, 14, 21, 28, 35, 42, and 56 days afterward, the locomotor functions were evaluated. A thermal radioluminescence apparatus (IITC, USA) was used to evaluate thermal hyperalgesia as previously described [25]. The mice were placed on a thermostatic platform for 30 min. A beam of strong light (working light intensity: 5%) was used to irradiate the plantar surface of the hind paw. Irradiation was terminated when positive actions were observed, such as rapid paw withdrawal or sudden hind paw licking. Repeated 3 times and record the irradiation times. The sensory functions were evaluated before the injury and 1, 3, 7, 14, 21, and 28 days afterward.

2.7. Neuroelectrophysiology analysis

We conducted neuroelectrophysiology analysis 56 days after the injury as previously described [26]. After the mice were anesthetized with 0.3% sodium pentobarbital intraperitoneally, the bregma was exposed and a stereotaxic device was used to position the electrodes. Stimulating electrodes were affixed to the skull's surface (1 mm caudal and 0.5 mm lateral, −4 mm caudal and 0.6 mm lateral to bregma, respectively). The contralateral hindlimb muscle was inserted with the recording electrodes. The reference electrode was positioned subcutaneously on the back. The motor-evoked potential (MEP) and latent period were recorded to evaluate neurological conductivity.

2.8. Tube formation and transwell migration

After starvation for 12 h, cells were digested with 0.25% trypsin (Gibco, United States), resuspended in FBS-free endothelial cell culture medium, and adjusted to a concentration of 80000/ml. Add 50 μl cold Matrigel (Corning, United States) into a 96-well plate, and spread the plate evenly to prevent the generation of bubbles. The plate was placed in the incubator for 30 min before adding 100 μl of the cell suspension to each well. To measure the impact of CSF-EVs on tube formation, 10 μg of EVs (sham-EVs or SCI-EVs) or an equal amount of PBS were added to each well after the cells had adhered. For transwell migration, transwell plates (Costar, United States) were used. Place 600 μl of culture medium (including 10% FBS) in the lower chamber and 100 μl of cell suspension in the upper chamber. After the cells had adhered, 10 μg of EVs (sham-EVs or SCI-EVs) or an equal amount of PBS was added into the culture medium as in the tube formation experiments above. Tube formation was pictured 6 h after intervention and migrated cells in the lower chamber were pictured 24 h after intervention using an optical microscope (Zeiss, Germany).

2.9. Scratch wound healing assay

To assess the capacity of bEnd.3 cells for horizontal migration, the scratch wound healing assay was applied. The cells were adjusted to a concentration of 150000/ml and suspended in growth media (10% FBS). Each well of a 6-well plate was seeded with 2 ml cell suspension. When the cells grew to confluence into a monolayer state, use a 200 μl pipette tip to draw the line straight. Then, change to an FBS-free culture medium after washing with PBS twice. To verify the effect of EVs on migration ability, 10 μg of EVs (sham-EVs or SCI-EVs) or the same amount of PBS were added to the culture medium. Images were captured at 0 and 12 h after adding EVs using an optical microscope (Zeiss, Germany).

2.10. Cell counting kit (CCK-8) assay

To evaluate the proliferation of bEnd.3 cells, the CCK-8 assay was employed. 100 μl of cell suspension was then put on a 96-well plate after adjusting the cell concentration to 50,000 cells per ml. To evaluate whether CSF-EVs could affect cell proliferation, 10 μg of EVs (sham-EVs or SCI-EVs) or PBS were added into the culture medium. After culturing for 24 h, 48 h, and 72 h, respectively, the cells were treated with 10 μl CCK-8 solution (MCE, United States) and cultured for additional 2 h. The microplate reader was used to assess the absorbance at 450 nm (Thermo Fisher Scientific, United States).

2.11. Western blot

RIPA buffer (Sigma, United States) and protease inhibitors (Sigma, United States) were applied for extracting the total protein. A BCA kit (Multi Science, China) was used to detect the protein concentration. 25 μg denatured proteins (containing 20% loading buffer) were subjected to a 10% gel. Adjust the voltage from 80 V to 120 V until the protein gradients were completely separated. Then, proteins were transferred from the gel to the PVDF membrane (Millipore, United States) by electroporation (300 A, 90 min). The bands were incubated with primary antibodies at 4° overnight after treating with 5% defatted milk. The following day, after washing with TBST (0.1% Tween) twice, the bands were transferred to secondary antibodies at room temperature for 2 h. After being subjected to ECL chemiluminescence (Millipore, United States) bands were visualized by a Bio-Rad Image Lab system (Bio-rad, United States). Actin was used as the internal reference. The antibodies used in this research were listed in Table 1.

2.12. Immunofluorescence staining

A 10 mm spinal segment containing the injury area was harvested and frozen sectioned into 14 μm slices. The slices were permeabilized with 0.1% PBST (Triton-X100) after being rinsed twice with PBS for 5 min. After blocking with 3% BSA, slices were incubated with primary antibodies overnight at 4°. For immunofluorescence staining of bEnd.3 cells, cell climbing sheets were fixed with 4% paraformaldehyde. After permeabilized with 0.1% PBST (Triton-X100) and blocked with 3% BSA solution, cells were incubated with CD31 antibody and Ki67 antibody overnight at 4°. The unbound antibodies were washed off the next day, and the secondary antibodies were incubated at room temperature for 1.5 h 4',6-diamidino2-phenylindole (DAPI) was used to stain the nucleus. The antibodies used in this research were listed in Table 1.

2.13. Hematoxylin-eosin staining

After perfusion, the bladders were collected and dehydrated with ethanol gradients. The bladder tissues were cut into 10-um sections. After

Table 1
Primary antibodies.

Antibodies	Application and Dilution	Catalog numbers and species
CD9	WB, 1:1000	Zenbio (380441, Rabbit)
CD81	WB, 1:1000	Abcam (ab217345, Rabbit)
Tsg101	WB, 1:1000	Abcam (ab125011, Rabbit)
p-AKT	WB, 1:750	Zen bio (381100, Rabbit)
AKT	WB, 1:750	Wanleibio (WL0003b, Rabbit)
Actin	WB, 1:50000	Proteintech (66009-1-Ig, Mouse)
CD31	IF, 1:200	R & D (FAB3628G-100, Goat)
Ki67	IF, 1:400	Huabio (HA721115, Rabbit)
Tuj-1	IF, 1:400	Abcam (ab18207, Rabbit)

gradient hydration, the tissue sections were treated with eosin dye for 5 min and hematoxylin dye for 15 s. After gradient dehydration, the sections were sealed with neutral balsam. A microscope (CKX41; Olympus Corporation, Tokyo, Japan) was used to obtain bladder wall images and Image J software was used to calculate detrusor muscle thickness.

2.14. Enzyme-linked immunosorbent assay (elisa)

TNF-α and IL-1β Elisa kits were used to evaluate the immunogenicity of pigs–SCI–EVs on mice. After collecting the supernatant of Raw264.7 cells treated by SCI-EVS and peripheral blood, add 100 ul samples or standard working solution to the ELISA plate, and incubate for 90 min at 37°. Then, discard the liquids, add 100 ul biotinylated antibody and incubate for 60 min at 37°. After washing with wash buffer, add 100 ul HRP conjugate and incubate for 30 min at 37°. 50ul substrates reagents were added and incubated for 15 min at 37° and stopped with stop solution. The microplate reader was used to assess the absorbance at 450 nm (Thermo Fisher Scientific, United States).

3. Statistics

The data were analyzed with GraphPad Prism 8. The threshold for statistical significance was $p < 0.05$. The data were presented as means ± standard deviations (SDs). The differences between the two groups were compared using an unpaired student's t-test. One-way ANOVA followed by Turkey's post hoc was used to compare the differences among multiple groups. At different time points, repeated-measures ANOVA was used to examine the differences in BMS scores or CCK-8 assay.

4. Results

4.1. CSF collection and CSF-EVs identification

As CSF content in a mouse is limited and the acquisition process is complex, we selected Bama miniature pigs to extract CSF-EVs at 7 days after SCI. As depicted in Fig. 1A, a lumbar puncture was used to obtain CSF 7 days after SCI. The EVs were extracted by ultracentrifugation (Fig. 1B). Western blot, NTA, and TEM were used to identify the CSF-EVs. Both EVs from sham-CSF and SCI-CSF displayed a spherical form with a double-membrane structure, according to the TEM images (Fig. 1C). According to the NTA, there was no discernible difference between the two EVs' diameter distributions, and the majority of the particles were distributed in the range of 20–300 nm (Fig. 1D). Western blot analysis indicated that both sham-EVs and SCI-EVs expressed the EVs surface markers including CD9, CD81, and Tsg101 (Fig. 1E). To evaluate whether SCI-EVs derived from Bama miniature pigs CSF could induce an immune reaction in mice, we tested TNF-α and IL-1β expression by Elisa. As shown in Fig. S1A, compared with the PBS-treated group, the TNF-α and IL-1β expression in the supernatant of Raw264.7 cells treated with SCI-EVs did not increase significantly. The in vivo experiments also showed that compared with the control group, the TNF-α and IL-1β expression in peripheral blood treated with SCI-EVs had no statistical difference (Fig. S1B).

4.2. SCI-EVs promoted proliferation and angiogenic activities of endothelial cells in vitro

To further determine whether EVs could be uptaken by endothelial cells, we labeled the EVs with PKH26 (Sigma, red), and added them into the culture medium of bEnd.3 cells. As shown in Fig. 2A, both sham-EVs and SCI-EVs were uptaken by bEnd.3 cells (stained by CD31, green). To explore the effect of sham-EVs and SCI-EVs on cell proliferation, we conducted CCK-8 analysis and immunofluorescence. CD31 (green) and Ki67 (red) immunofluorescence labeling revealed that SCI-EVs may greatly boost bEnd.3 cells' capacity for proliferation (Fig. 2B and C). The CCK-8 test also showed that SCI-EVs have enhanced cell proliferation capabilities (Fig. 2D). Both sham-EVs and SCI-EVs increased branch numbers and segment lengths when compared to the PBS-treated group, and SCI-EVs were more effective in promoting tubes forming than that with the application of sham-EVs (Fig. 2E and H). Transwell migration studies demonstrated that the addition of SCI-EVs significantly improved the migration capacity of bEND.3 cells (Fig. 2F and I). The scratch wound healing experiment revealed a similar tendency, with a higher migration rate after the addition of SCI-EVs (Fig. 2G and J). These findings showed

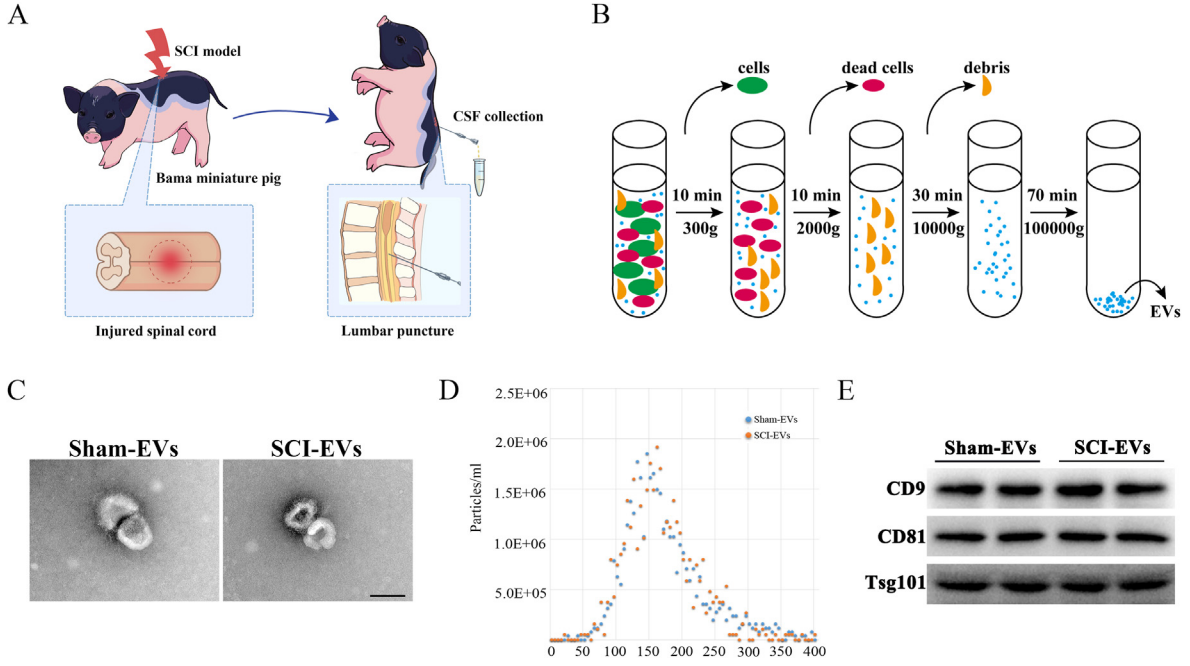

Fig. 1. CSF collection and CSF-EVs identification (A) Schematic depiction of CSF collection from pigs (B) CSF-EVs purification by ultracentrifugation (C) Transmission electron microscope (TEM) images of sham-EVs and SCI-EVs. Scale bar: 100 nm (D) Nano-tracking analysis (NTA) of sham-EVs and SCI-EVs (E) Western blot analysis of surface markers CD9, CD81, and Tsg101.

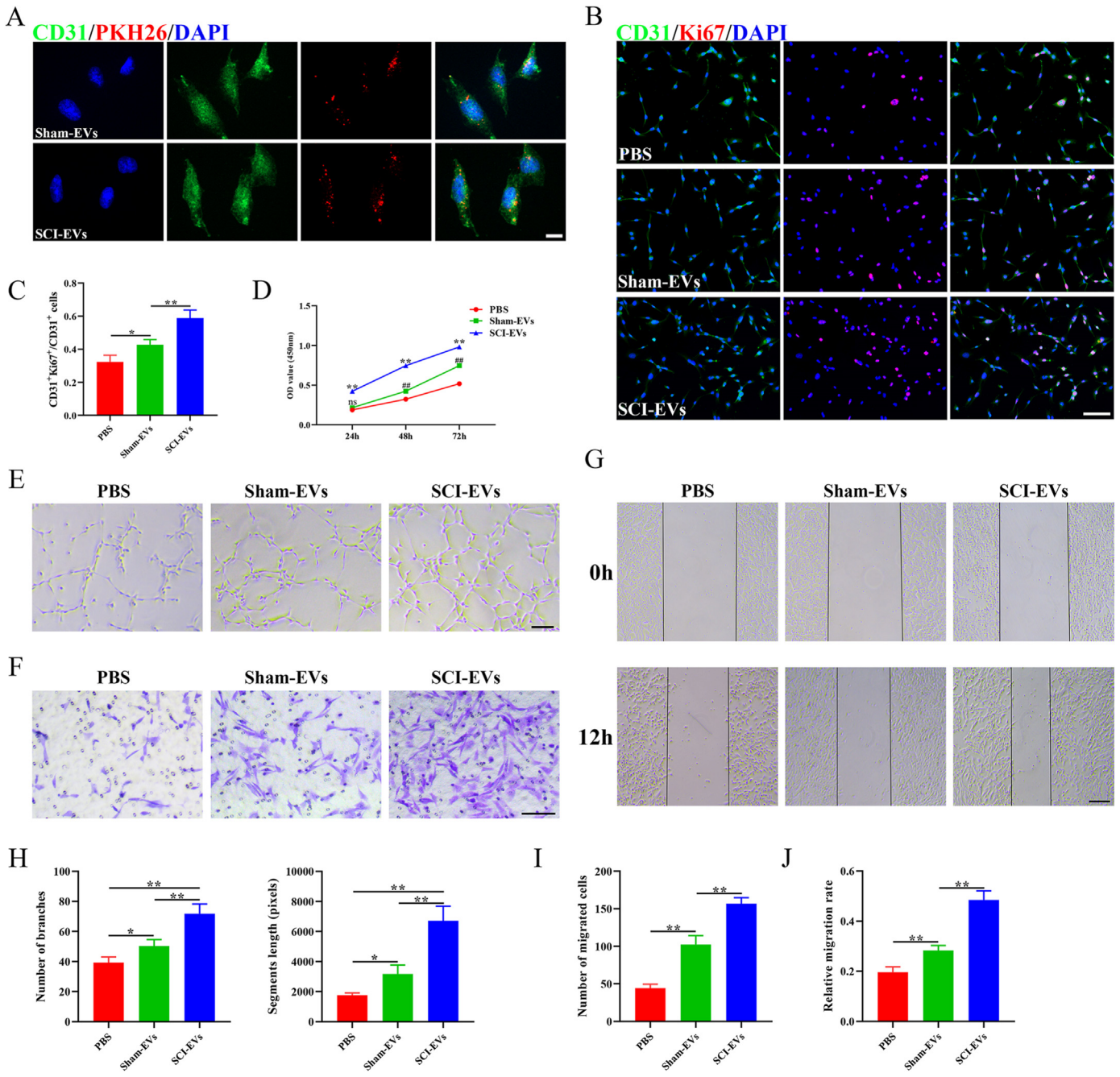

Fig. 2. SCI-EVs promoted proliferation and function of endothelial cells in vitro (A) Representative fluorescent images of CD31 (Green) and PKH26 (Red) in Sham-EVs and SCI-EVs treated group. Scale bar: 20 μm (B) Representative fluorescent images of CD31 (green) and Ki67 (red) in PBS, sham-EVs, and SCI-EVs treated groups. Scale bar: 100 μm (C) Quantification of the ratio of $CD31^{+}Ki67^{+}/CD31^{+}$. n = 4 per group (D) CCK-8 assay for cell proliferation in PBS, sham-EVs, SCI-EVs treated groups. n = 3 per group (E) Representative images of bEnd.3 canaliculization in PBS, sham-EVs, SCI-EVs treated groups. Scale bar: 100 μm (F) Representative images of bEnd.3 transwell migration in PBS, sham-EVs, SCI-EVs treated groups. Scale bar: 100 μm (G) Representative images of the horizontal migration of bEnd.3 in PBS, sham-EVs, SCI-EVs treated groups. Scale bar: 200 μm (H) Quantification of branch number and segment length in (E). n = 4 per group (I) Quantification of the number of migrated cells in (F). n = 4 per group (J) Quantification of relative migration rate in (G). n = 4 per group. The data are presented as the means ± SD. *p < 0.05, **p < 0.01 compared among the different treatment groups. (For interpretation of the references to color in this figure legend, the reader is referred to the Web version of this article.)

that SCI-EVs increased endothelial cell proliferation and angiogenic activities.

4.3. SCI-EVs facilitated neurological function recovery after SCI

We combined DiR-labeled EVs or PKH26-labeled EVs with hydrogels and applied them to the damaged spinal cord to see if SCI-EVs may have an impact on neurological function following SCI (Fig. 3A). As shown in Fig. S2A, the hydrogel has a porous structure. The hydrogel degraded continuously. After 28 days, the hydrogel degraded by about 25% (Fig. S2B), which was in consistent with a previous study [27]. Both sham-EVs and SCI-EVs (labeled by DiR), according to the results of in vivo imaging, might be released for 28 days (Fig. 3B and C). The immunofluorescence staining indicated that PKH26-labeled EVs could be

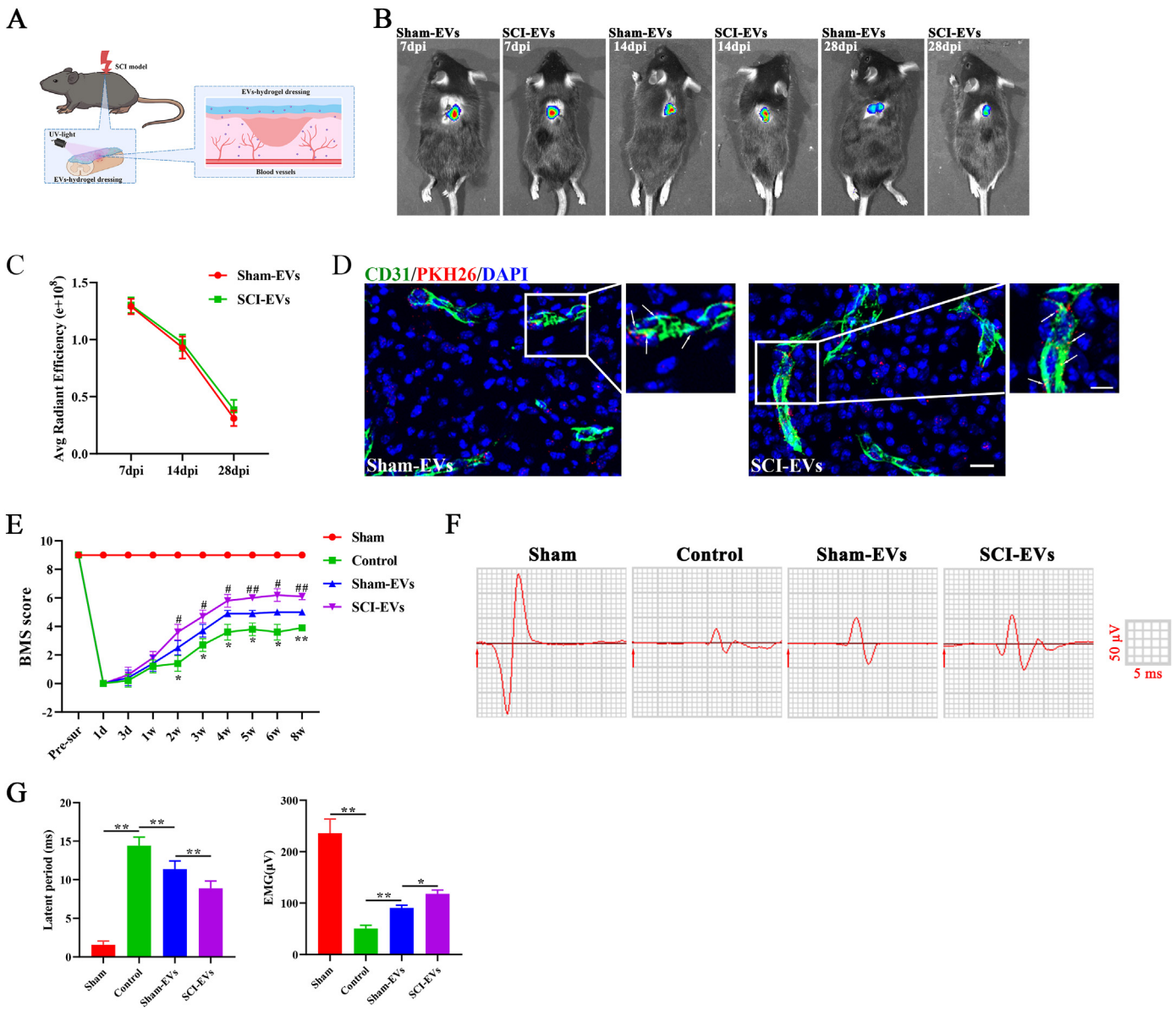

Fig. 3. SCI-EVs facilitated neurological function recovery (A) Schematic depiction of EVs-hydrogel dressing (B) In vivo tracing of DiR-labeled sham-EVs and SCI-EVs embedded in hydrogels in the injured spinal cord at 7-, 14- and 28 days after SCI (C) Quantification of average radiation efficiency in (B). n = 3 per group (D) Representative fluorescent images of CD31 (Green) and PKH26 (Red) in sham-EVs and SCI-EVs treated groups. The white arrow indicated EVs ingested by endothelial cells. Scale bar: 20 μm. Scale bar for magnified images: 10 μm (E) BMS scores at different time points of sham, control, sham-EVs, and SCI-EVs treated groups. n = 5 per group (F) Neuroelectrophysiology analysis of sham, control, sham-EVs, and SCI-EVs treated groups at 56 days post-SCI (G) Quantification of latent period and motor evoked potential in (E). n = 5 per group. The data are presented as the means ± SD. *p < 0.05, **p < 0.01 compared among the different treatment groups. (For interpretation of the references to color in this figure legend, the reader is referred to the Web version of this article.)

ingested by endothelial cells (CD31, green) (Fig. 3D). Compared to the PBS and sham-EVs treated groups, the SCI-EVs treated mice had better-enhanced locomotor function from 2 weeks following injury until observation endpoint (Fig. 3E). As shown in Fig. S3A, compared to the PBS and sham-EVs treated groups, the SCI-EVs treated mice had better sensory function recovery from 7 days after SCI until observation endpoint. The detrusor muscle in SCI-EVs treated mice was thicker than in PBS and sham-EVs treated groups 28 days after injury, indicating a better urination function (Figs. S3B–C). Neuroelectrophysiology analysis was used to assess neural conduction after SCI. As shown in Fig. 3F and G, compared to PBS treated group, sham-EVs and SCI-EVs treated mice exhibited shorter latent periods and higher motor evoked potentials, whereas, the effect of SCI-EVs on promoting neural conductivity was more obvious. Axonal regrowth is essential for the recovery of neurological function [25]. Both sham-EVs and SCI-EVs promoted axonal regrowth after SCI. Compared to the sham-EVs treated group, mice in SCI-EVs treated group showed higher axon density, as shown by Tuj-1 staining (Fig. S4). Together, these results suggested that SCI-EVs could facilitate neurological function recovery after SCI.

4.4. SCI-EVs promoted vascular regeneration after SCI in vivo

We used immunofluorescence to stain blood vessels to further investigate if EVs could improve vascular regeneration in vivo. According to the findings, both sham-EVs and SCI-EVs significantly enhanced the vessel densities in mice, and SCI-EVs had a greater impact on vascular regeneration (Fig. 4A and B). To assess the percentage of proliferating endothelial cells, we additionally co-stained CD31 (green) and Ki67

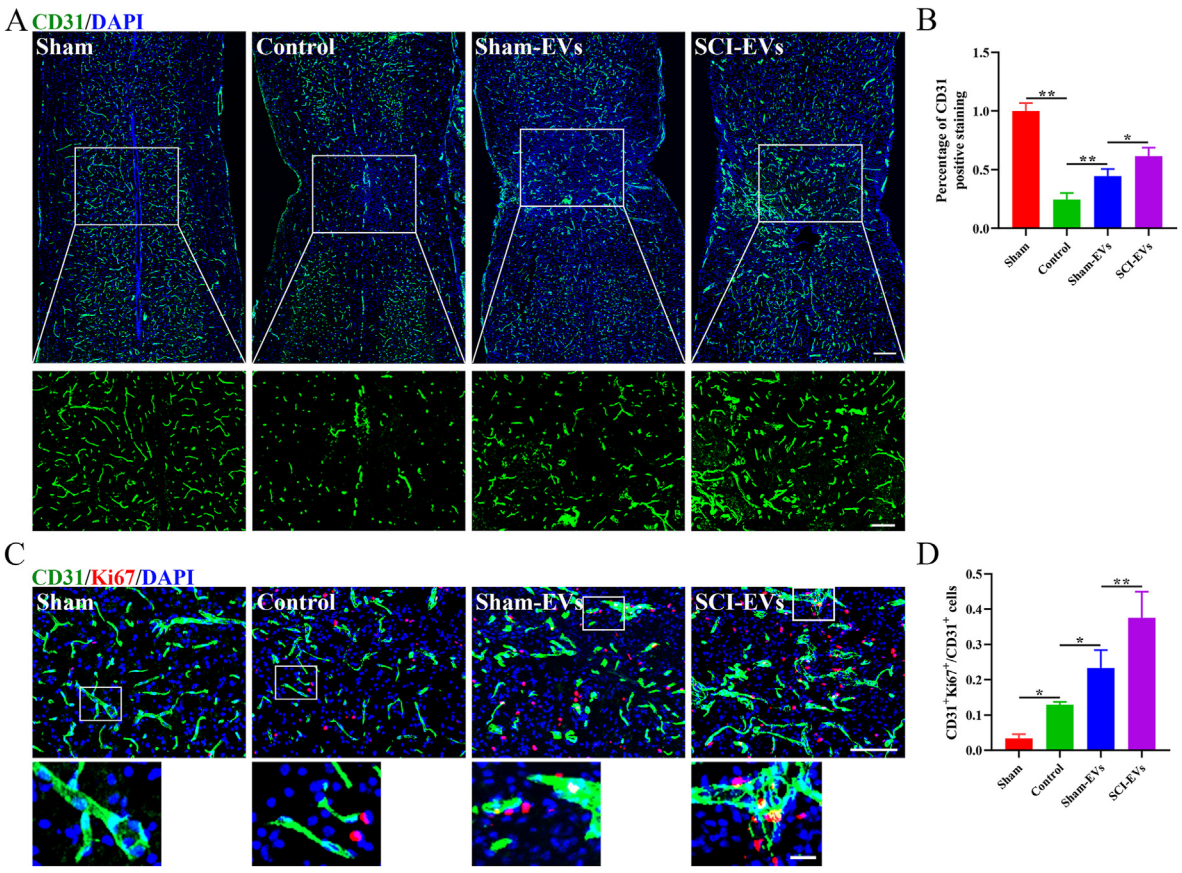

Fig. 4. SCI-EVs promoted vascular regeneration in vivo after SCI (A) Representative immunofluorescence images of CD31 (Green) in sham, control, sham-EVs, and SCI-EVs treated groups. Scale bar: 200 μm. In the lower panel are magnified images of the boxed area. Scale bar: 100 μm (B) Quantification of percentages of CD31 positive staining in (A). n = 4 per group (C) Representative immunofluorescence images of CD31 (green) and Ki67 (Red) in sham, control, sham-EVs, and SCI-EVs treated groups. Scale bar: 100 μm. Scale bar for magnified images: 20 μm (D) Quantification of the ratio of $CD31^{+}Ki67^{+}/CD31^{+}$ cells in (C). n = 4 per group. The data are presented as the means ± SD. *p < 0.05, **p < 0.01 compared among the different treatment groups. (For interpretation of the references to color in this figure legend, the reader is referred to the Web version of this article.)

(red). SCI-EVs and sham-EVs both raised the proportion of $CD31^{+}Ki67^{+}$ cells. SCI-EVs showed a higher impact on endothelial cell proliferation as compared to the group that received sham-EV treatment (Fig. 5C and D). These results indicated that SCI-EVs could promote vascular regeneration.

4.4.1. *SCI-EVs promoted proliferation and function of endothelial cells by activating PI3K/AKT pathway*

PI3K/AKT pathway was closely related to angiogenesis after SCI [28]. To determine if the PI3K/AKT pathway was involved in the process of EVs to stimulate angiogenesis, we used the PI3K inhibitor LY294002 (20 μM, MedChemExpress, United States). Western blot analysis revealed that the group treated with SCI-EVs could enhance the expression of p-AKT (Fig. 5A and B), while LY294002 attenuate the positive effect of SCI-EVs on activation of PI3K/AKT pathway (Fig. 5C and D). SCI-EVs were able to dramatically increase the proportion of $Ki67^{+}$ cells, as seen in Fig. 5E and F, however, LY294002 attenuated this effect on cell proliferation. Tube formation analysis indicated that blocking PI3K/AKT pathway with LY294002 could attenuate the tube-forming ability of SCI-EVs (Fig. 5G and J). Similar patterns were seen in the transwell migration and scratch wound healing investigations. When treated with SCI-EVs + LY294002, compared to the SCI-EVs treated group, the number of cells that migrated to the bottom chamber and the horizontal migration distance were reduced (Fig. 5H and I, 5 K-L). These findings suggested that SCI-EVs stimulated the PI3K/AKT pathway, which in turn increased endothelial cell proliferation and angiogenic activities in vitro.

LY294002 administration attenuated the effects of SCI-EVs on vascular regeneration and functional recovery after SCI.

To determine if SCI-EVs affected vascular regeneration and function recovery by activating the PI3K-AKT pathway in vivo, PI3K inhibitor LY294002 was injected intraperitoneally twice per week for four consecutive weeks at a dose of 25 mg/kg. Western blot analysis indicated that SCI-EVs elevated p-AKT expression, while LY294002 reduced this effect (Fig. 6A). According to the BMS score, LY294002 lessened the impact of SCI-EVs in improving motor function. Mice in the SCI-EVs group showed better recovery in motor function than mice in the SCI-EVs + LY294002 treated group from the third week to the end of the observation period (Fig. 6B). As shown in Fig. S5A, LY294002 reduced the positive effect of SCI-EVs on sensory function recovery from 7 days after SCI until observation endpoint. SCI-EVs significantly increased the detrusor muscle thickness, while LY294002 reduced this effect (Fig. S5B). Electrophysiological studies showed that 56 days after injury, mice in the SCI-EVs + LY294002 treated group displayed impaired neurological conduction, with longer latent periods and lower motor evoked potentials than animals in the SCI-EVs treated group (Fig. 6C and D). SCI-EVs increased vessel densities in the spinal cord after injury, according to CD31 staining data, while LY294002 lessened their impact on vascular regeneration (Fig. 6E and F). We co-stained CD31 (green) and Ki67 (red) to see if LY294002 affected the proliferation of endothelial cells in the injured spinal cord. Treatment with SCI-EVs raised the ratio of $CD31^{+}Ki67^{+}$ cells, but treatment with LY294002 significantly decreased the amount of $CD31^{+}Ki67^{+}$ cells in the injured spinal cord (Fig. 6G and

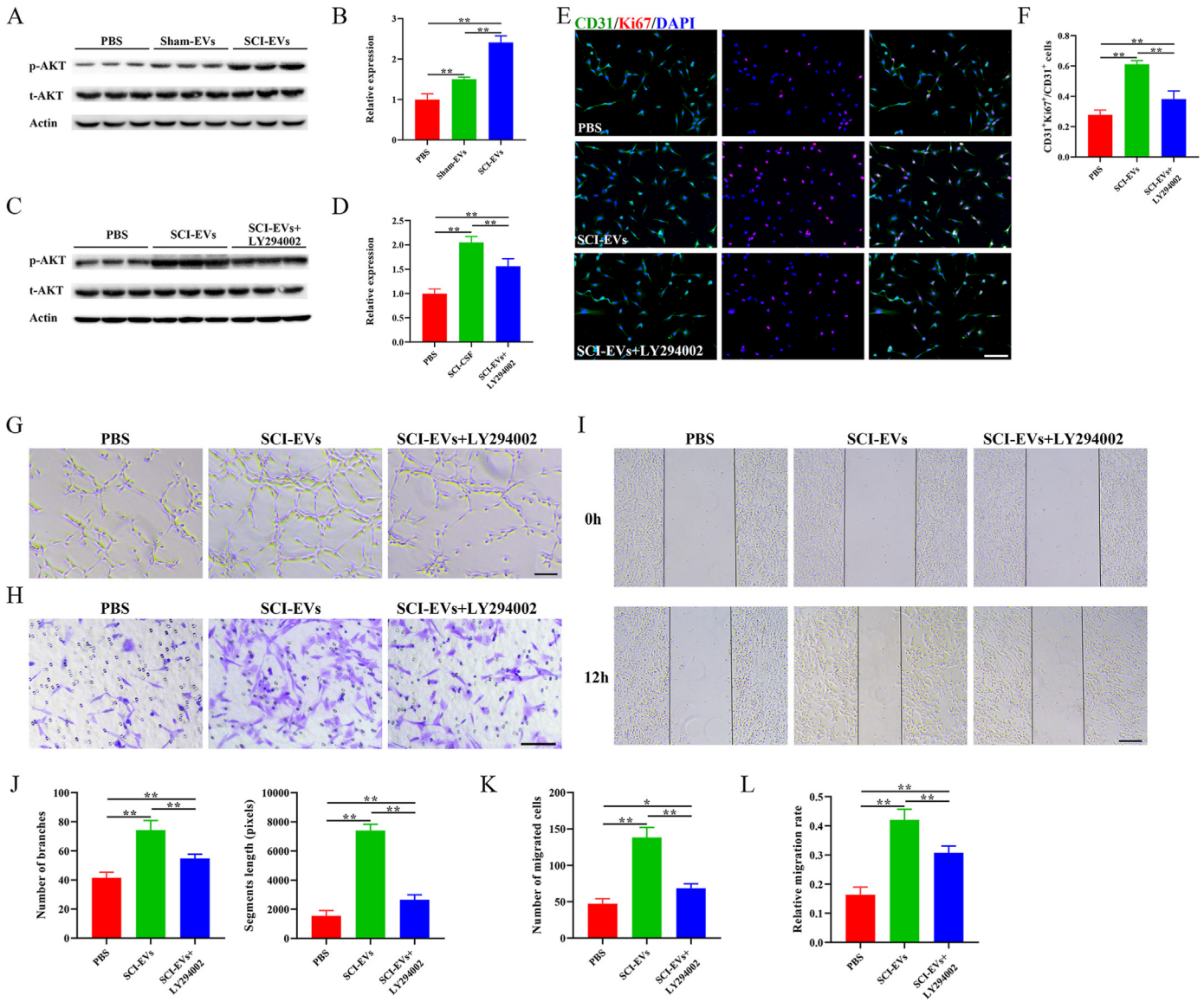

Fig. 5. SCI-EVs promoted proliferation and function of endothelial cells in vitro by activating PI3K/AKT pathway (A) Western blot analysis of p-AKT, AKT, and Actin expression in PBS, sham-EVs, and SCI-EVs treated group (B) Quantification of protein expression in (A). n = 3 per group (C) Western blot analysis of p-AKT, AKT, and Actin expression in PBS, SCI-EVs, and SCI-EVs + LY294002 treated group (D) Quantification of protein expression in (C). n = 3 per group (E) Representative fluorescent images of CD31 (green) and Ki67 (red) in PBS, SCI-EVs, and SCI-EVs + LY294002 treated group. Scale bar: 100 μm (F) Quantification of the ratio of $CD31^{+}Ki67^{+}/CD31^{+}$. n = 4 per group (G) Representative images of bEnd.3 canaliculization in PBS, SCI-EVs, and SCI-EVs + LY294002 treated group. Scale bar: 100 μm (H) Representative images of bEnd.3 transwell migration in PBS, SCI-EVs, and SCI-EVs + LY294002 treated group. Scale bar: 100 μm (I) Representative images of the horizontal migration in PBS, SCI-EVs, and SCI-EVs + LY294002 treated group. Scale bar: 200 μm (J) Quantification of branch number and segment length in (G). n = 4 per group (K) Quantification of the number of migrated cells in (H). n = 4 per group (L) Quantification of relative migration rate in (I). n = 4 per group. The data are presented as the means ± SD. *p < 0.05, **p < 0.01 compared among the different treatment groups. (For interpretation of the references to color in this figure legend, the reader is referred to the Web version of this article.)

H). These findings revealed that SCI-EVs promoted vascular regeneration and function recovery via enhanced PI3K-AKT pathway activation in vivo.

5. Discussion

SCI results in temporary or permanent changes in CNS function. In recent years, the incidence of SCI has been on the rise worldwide, bringing a heavy burden to patients and their families [29,30]. The initial mechanical injury (primary injury) is often accompanied by damage to the vascular network and disruption of the BSCB and initiates a secondary injury cascade leading to progressive spinal cord dysfunction [1,4]. The integrity of the vascular network is critical for regulating nutrient, oxygen, and metabolite balance, which is essential for the maintenance of homeostasis of the spinal cord [31]. To promote the regeneration of new blood vessels, many strategies have been developed. Specifically, EVs can be used as drug carriers to simultaneously load multiple factors to promote angiogenesis [32]. In this study, we confirmed that CSF-EVs isolated from the subarachnoid space of pigs with SCI may have angiogenic factors and promote vascular regeneration and neurological recovery after SCI through the PI3K/AKT signaling pathway, which may provide a new potential therapeutic strategy for the treatment of SCI.

EVs can be secreted by multiple cells and are essential for intercellular communication, and is able to either target neighbor cells or travel to distant organs and tissues [13]. EVs are double-membrane structures

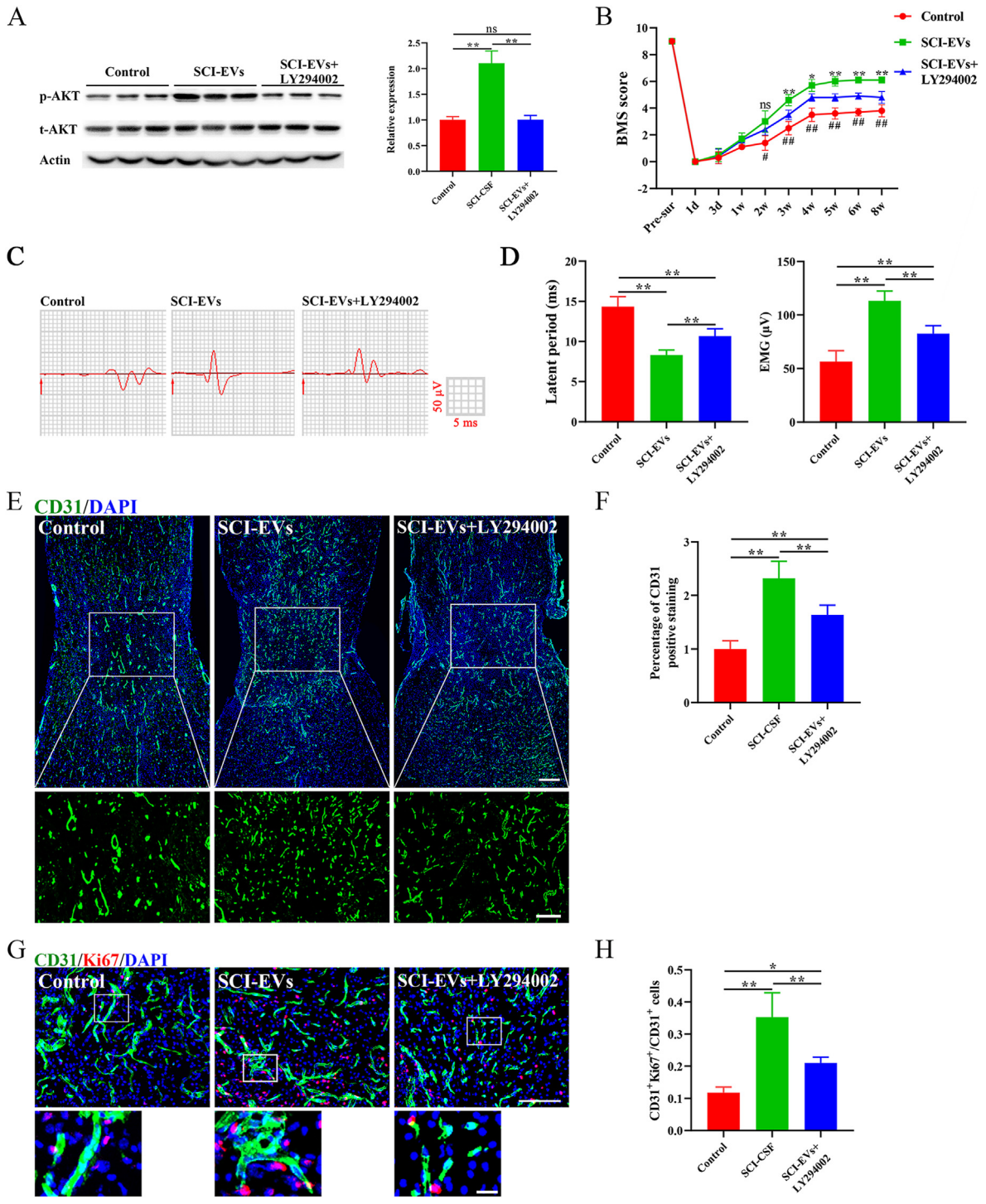

Fig. 6. SCI-EVs enhanced neurological function and vascular regeneration by activating the PI3K-AKT pathway (A) Western blot analysis and quantification of p-AKT, AKT, and Actin expression in control, SCI-EVs, and SCI-EVs + LY294002 treated group. n = 3 per group (B) BMS scores at different time points of control, SCI-EVs, and SCI-EVs + LY294002 treated groups. n = 5 per group (C) Neuroelectrophysiology analysis of control, SCI-EVs, and SCI-EVs + LY294002 treated groups at 56 days post-SCI (D) Quantification of latent period and motor evoked potential in (C). n = 5 per group (E) Representative immunofluorescence images of CD31 (Green) in control, SCI-EVs, and SCI-EVs + LY294002 treated groups. Scale bar: 200 μm. In the lower panel are magnified images of the boxed area. Scale bar: 100 μm (F) Quantification of percentages of CD31 positive staining in (E). n = 4 per group (G) Representative immunofluorescence images of CD31 (green) and Ki67 (Red) in control, SCI-EVs, and SCI-EVs + LY294002 treated groups. Scale bar: 100 μm. Scale bar for magnified images: 20 μm (H) Quantification of the ratio of $CD31^{+}Ki67^{+}/CD31^{+}$ cells in (G). n = 4 per group. The data are presented as the means ± SD. *p < 0.05, **p < 0.01 compared among the different treatment groups. (For interpretation of the references to color in this figure legend, the reader is referred to the Web version of this article.)

with diameters ranging from 40 to 150 nm and exist in body fluids such as serum, urine, tears, and cerebrospinal fluid [33]. Different from cells, the immunogenicity of EVs, even from different species, was very limited. Many studies have used EVs derived from xenogeneic cells (such as human umbilical cord mesenchymal stem cells and human urine-derived stem cells) to treat SCI in mice, and it has been confirmed that there is almost no immunogenicity [17,34]. In our research, we also proved that pig CSF-derived EVs did not produce significant inflammatory response in mice. The EV cargo is rich in proteins, lipids, and microRNAs, which can be transferred to recipient cells [35]. The abnormal generation of EVs in cerebrospinal fluid is often caused by disorders of the CNS and is a relatively stable source of disease biomarkers, which can be used to evaluate the severity and prognosis of the disease [36]. A microRNA sequencing revealed that miR-130 b-3p and miR-501–5p in CSF-EVs are involved in the etiology of congenital hydrocephalus [37]. Xu et al. confirmed that the high expression of miR-3184–3p in glioma patient CSF-EVs could promote the M2 polarization of macrophages by targeting PDCD4 and accelerate the progression of glioma [38]. EVs secreted by various cell resources have been proved to play an active role in promoting functional repair after SCI [39]. As spinal cord is surrounded and protected by CSF, the changes of CSF components could reflect the physiological or pathological state of the spinal cord [40]. Compared with EVs derived from stem cells or other body fluids, CSF-EVs may have a close relationship with neurological functional recovery following SCI. Some protective factors secreted by spinal cord cells will be released into CSF in a form of EVs, thus promoting the neurological function after SCI. However, the alteration of CSF-EVs content in mice or patients have not been explored. How to obtain large volumes of CSF to collect EVs is also a huge challenge. It has been reported that CSF-generated EVs enhanced neuronal survival and reduce neuronal apoptosis in vitro [22]. However, whether CSF-EVs affect angiogenesis and neurological function after SCI, remains unknown. In the present study, we found for the first time that SCI-CSF-EVs were more favorable than sham–CSF–EVs in promoting vascular regeneration and neurological recovery. The effects of EVs are largely determined by their contents, which vary in response to specific physiological or pathological circumstances [41]. We suspected that due to the self-protection mechanism of the spinal cord, more favorable factors will be released into the CSF in the form of EVs after SCI, making SCI-CSF-EVs more capable of promoting the functional recovery than sham–CSF–EVs. However, more studies are needed to determine the differences in the molecular composition of CSF between the sham–CSF–EVs and SC-CSF-EVs.

One of the traditional signaling pathways that control angiogenesis is the phosphoinositide 3-kinase/AKT (PI3K/AKT) pathway [42]. When PI3K is paired with elements such as growth hormone or insulin, it can stimulate the phosphorylation of AKT, which further regulates the expression of downstream genes [43]. A substance known as HQ-1H, or plant extracts known as ginsenosides, has been shown to enhance angiogenesis after ischemic stroke by stimulating the PI3K/AKT pathway, which is essential for neuron repair [44,45]. The PI3K/AKT signaling pathway is also crucial for neurological functional recovery following spinal cord damage. Olfactory ensheathing cells (OECs) had a pro-angiogenic role in a PI3K/AKT-dependent manner and can successfully induce angiogenesis and improve the local microenvironment of spinal cord lesions [28]. Furthermore, according to one of our recent studies, EVs made from human urinary stem cells (HUSC) were able to transport Agnptl3 to endothelial cells, activate the PI3K/AKT pathway, and promote angiogenesis after SCI [17]. In addition to affecting angiogenesis after SCI, the PI3K/AKT pathway also plays other roles, such as inducing macrophage polarization to M2 type to reduce local inflammation or promoting microglial proliferation [46,47]. Other signal pathways were also involved in vascular regeneration after SCI. M2 macrophages derived exosomes activated wnt/β-catenin pathway to promote vascular regeneration after SCI by transferring ubiquitin thioesterase otulin (OTULIN) to endothelial cells [16]. Another study showed HIF-1α/VEGF pathway improved angiogenesis and functional recovery [48]. In our study, CSF-EVs stimulated angiogenesis by activating the PI3K/AKT signaling pathway. The PI3K inhibitor LY294002 partially blocked the pro-angiogenic effect of CSF-EVs on vascular endothelial cells, suggesting that there may be more underlying processes involved in the promotion of angiogenesis.

Our study has a few drawbacks as well. First, although we were able to determine that CSF-EVs might increase angiogenesis and axon regrowth, it was unclear whether they could also influence vascular permeability or local inflammatory responses. Second, due to the lack of high-throughput sequencing of CSF-EVs, we were unable to identify the factors that mediate the role of EVs in increasing angiogenesis.

In conclusion, we found that CSF-EV derived from the subarachnoid space after SCI can promote angiogenesis by activating the PI3K/AKT pathway and improve neurological function after SCI, which may provide a new potential therapy for the management of SCI.

Author contributions

YC, CD and JH designed the study. CL and YJ carried out most of the experiments and data analysis. TQ and FY assisted in experiments and data analysis. CL and YJ drafted the manuscript. YC, CD and JH revised the manuscript. All authors contributed to the manuscript.

Funding

This work was funded by the National Natural Science Foundation of China (grant 81902224, 82030071 and 82272495), the Natural Science Foundation of Hunan Province (grant 2020JJ4874), the Science and Technology Major Project of Changsha (kh2103008) and the Fundamental Research Funds for the Central Universities of Central South University (2022ZZTS0943).

Declaration of competing interest

The authors have no conflicts of interest relevant to this article.

Appendix A. Supplementary data

Supplementary data to this article can be found online at https://doi.org/10.1016/j.jot.2023.02.001.

References

[1] Ahuja CS, Wilson JR, Nori S, Kotter MRN, Druschel C, Curt A, et al. Traumatic spinal cord injury. Nat Rev Dis Prim 2017;3:17018 [eng].
[2] Rubiano AM, Carney N, Chesnut R, Puyana JC. Global neurotrauma research challenges and opportunities. Nature 2015;527(7578):S193–7 [eng].
[3] Dray C, Rougon G, Debarbieux F. Quantitative analysis by in vivo imaging of the dynamics of vascular and axonal networks in injured mouse spinal cord. Proc. Natl. Acad. Sci. U.S.A 2009;106(23):9459–64 [eng].
[4] Yao Y, Xu J, Yu T, Chen Z, Xiao Z, Wang J, et al. Flufenamic acid inhibits secondary hemorrhage and BSCB disruption after spinal cord injury. Theranostics 2018;8(15):4181–98 [eng].
[5] Lun MP, Monuki ES, Lehtinen MK. Development and functions of the choroid plexus-cerebrospinal fluid system. Nat Rev Neurosci 2015;16(8):445–57 [eng].
[6] Brinkmalm A, Brinkmalm G, Honer WG, Frölich L, Hausner L, Minthon L, et al. SNAP-25 is a promising novel cerebrospinal fluid biomarker for synapse degeneration in Alzheimer's disease. Mol Neurodegener 2014;9:53 [eng].
[7] Nilsson J, Ashton NJ, Benedet AL, Montoliu-Gaya L, Gobom J, Pascoal TA, et al. Quantification of SNAP-25 with mass spectrometry and Simoa: a method comparison in Alzheimer's disease. Alzheimer's Res Ther 2022;14(1):78 [eng].
[8] Židó M, Kačer D, Valeš K, Svobodová Z, Zimová D, Štětkárová I. Metabolomics of cerebrospinal fluid in multiple sclerosis compared with healthy controls: a pilot study. Front Neurol 2022;13:874121 [eng].
[9] Skinnider MA, Rogalski J, Tigchelaar S, Manouchehri N, Prudova A, Jackson AM, et al. Proteomic portraits reveal evolutionarily conserved and divergent responses to spinal cord injury. Mol Cell Proteomics 2021;20:100096 [eng].
[10] Stukas S, Gill J, Cooper J, Belanger L, Ritchie L, Tsang A, et al. Characterization of cerebrospinal fluid ubiquitin C-terminal hydrolase L1 as a biomarker of human acute traumatic spinal cord injury. J Neurotrauma 2021;38(15):2055–64 [eng].
[11] Tigchelaar S, Gupta R, Shannon CP, Streijger F, Sinha S, Flibotte S, et al. MicroRNA biomarkers in cerebrospinal fluid and serum reflect injury severity in human acute traumatic spinal cord injury. J Neurotrauma 2019;36(15):2358–71 [eng].

[12] Grange C, Bussolati B. Extracellular vesicles in kidney disease. Nat Rev Nephrol 2022 [eng].
[13] van Niel G, Carter DRF, Clayton A, Lambert DW, Raposo G, Vader P. Challenges and directions in studying cell-cell communication by extracellular vesicles. Nat Rev Mol Cell Biol 2022;23(5):369–82 [eng].
[14] Gregorius J, Wang C, Stambouli O, Hussner T, Qi Y, Tertel T, et al. Small extracellular vesicles obtained from hypoxic mesenchymal stromal cells have unique characteristics that promote cerebral angiogenesis, brain remodeling and neurological recovery after focal cerebral ischemia in mice. Basic Res Cardiol 2021;116(1):40 [eng].
[15] Peng W, Wan L, Luo Z, Xie Y, Liu Y, Huang T, et al. Microglia-derived exosomes improve spinal cord functional recovery after injury via inhibiting oxidative stress and promoting the survival and function of endothelia cells. Oxid Med Cell Longev 2021;2021:1695087 [eng].
[16] Luo Z, Peng W, Xu Y, Xie Y, Liu Y, Lu H, et al. Exosomal OTULIN from M2 macrophages promotes the recovery of spinal cord injuries via stimulating Wnt/β-catenin pathway-mediated vascular regeneration. Acta Biomater 2021;136:519–32 [eng].
[17] Cao Y, Xu Y, Chen C, Xie H, Lu H, Hu J. Local delivery of USC-derived exosomes harboring ANGPTL3 enhances spinal cord functional recovery after injury by promoting angiogenesis. Stem Cell Res Ther 2021;12(1):20 [eng].
[18] Thompson AG, Gray E, Heman-Ackah SM, Mäger I, Talbot K, Andaloussi SE, et al. Extracellular vesicles in neurodegenerative disease - pathogenesis to biomarkers. Nat Rev Neurol 2016;12(6):346–57 [eng].
[19] Quesenberry PJ, Aliotta J, Deregibus MC, Camussi G. Role of extracellular RNA-carrying vesicles in cell differentiation and reprogramming. Stem Cell Res Ther 2015;6:153 [eng].
[20] Lai H, Li Y, Zhang H, Hu J, Liao J, Su Y, et al. exoRBase 2.0: an atlas of mRNA, lncRNA and circRNA in extracellular vesicles from human biofluids. Nucleic Acids Res 2022;50(D1):D118–28 [eng].
[21] Caldi Gomes L, Roser A-E, Jain G, Pena Centeno T, Maass F, Schilde L, et al. MicroRNAs from extracellular vesicles as a signature for Parkinson's disease. Clin Transl Med 2021;11(4):e357 [eng].
[22] Kong F-L, Wang X-P, Li Y-N, Wang H-X. The role of exosomes derived from cerebrospinal fluid of spinal cord injury in neuron proliferation in vitro. Artif Cell Nanomed Biotechnol 2018;46(1):200–5 [eng].
[23] Li C, Qin T, Zhao J, He R, Wen H, Duan C, et al. Bone marrow mesenchymal stem cell-derived exosome-educated macrophages promote functional healing after spinal cord injury. Front Cell Neurosci 2021;15:725573 [eng].
[24] Basso DM, Fisher LC, Anderson AJ, Jakeman LB, McTigue DM, Popovich PG. Basso Mouse Scale for locomotion detects differences in recovery after spinal cord injury in five common mouse strains. J Neurotrauma 2006;23(5):635–59 [eng].
[25] Guo Z, Li C, Cao Y, Qin T, Jiang L, Xu Y, et al. UTX/KDM6A deletion promotes the recovery of spinal cord injury by epigenetically triggering intrinsic neural regeneration. Mol Ther Methods Clin Dev 2021;20:337–49 [eng].
[26] Schlag MG, Hopf R, Redl H. Serial recording of sensory, corticomotor, and brainstem-derived motor evoked potentials in the rat. SMR (Somatosens Mot Res) 2001;18(2):106–16 [eng].
[27] Liu D, Shen H, Shen Y, Long G, He X, Zhao Y, et al. Dual-cues laden scaffold facilitates neurovascular regeneration and motor functional recovery after complete spinal cord injury. Adv Healthc Mater 2021;10(10):e2100089 [eng].
[28] Wang X, Jiang C, Zhang Y, Chen Z, Fan H, Zhang Y, et al. The promoting effects of activated olfactory ensheathing cells on angiogenesis after spinal cord injury through the PI3K/Akt pathway. Cell Biosci 2022;12(1):23 [eng].
[29] James Spencer L, Theadom Alice, Ellenbogen Richard G, Bannick Marlena S, Montjoy-Venning Wcliff, Lucchesi Lydia R, et al. GBD 2016 Traumatic Brain Injury and Spinal Cord Injury Collaborators. Global, regional, and national burden of traumatic brain injury and spinal cord injury, 1990-2016: a systematic analysis for the Global Burden of Disease Study 2016. Lancet Neurol 2019 Jan;18(1):56–87.
[30] Feigin Valery L, Nichols Emma, Alam Tahiya, Bannick Marlena S, Beghi Ettore, Blake Natacha, et al. Global, regional, and national burden of neurological disorders, 1990-2016: a systematic analysis for the Global Burden of Disease Study 2016. Lancet Neurol 2019;18(5):459–80.
[31] Yao C, Cao X, Yu B. Revascularization after traumatic spinal cord injury. Front Physiol 2021;12:631500 [eng].
[32] Todorova D, Simoncini S, Lacroix R, Sabatier F, Dignat-George F. Extracellular vesicles in angiogenesis. Circ Res 2017;120(10):1658–73 [eng].
[33] Sahebi R, Langari H, Fathinezhad Z, Bahari Sani Z, Avan A, Ghayour Mobarhan M, et al. Exosomes: new insights into cancer mechanisms. J Cell Biochem 2020;121(1) [eng].
[34] Kang J, Guo Y. Human umbilical cord mesenchymal stem cells derived exosomes promote neurological function recovery in a rat spinal cord injury model. Neurochem Res 2022;47(6):1532–40 [eng].
[35] Isaac R, Reis FCG, Ying W, Olefsky JM. Exosomes as mediators of intercellular crosstalk in metabolism. Cell Metabol 2021;33(9):1744–62 [eng].
[36] Doroszkiewicz J, Groblewska M, Mroczko B. Molecular biomarkers and their implications for the early diagnosis of selected neurodegenerative diseases. Int J Mol Sci 2022;23(9) [eng].
[37] Chen S, Li H, Zheng J, Hao L, Jing T, Wu P, et al. Expression profiles of exosomal MicroRNAs derived from cerebrospinal fluid in patients with congenital hydrocephalus determined by MicroRNA sequencing. Dis Markers 2022;2022:5344508 [eng].
[38] Xu H, Li M, Pan Z, Zhang Z, Gao Z, Zhao R, et al. miR-3184-3p enriched in cerebrospinal fluid exosomes contributes to progression of glioma and promotes M2-like macrophage polarization. Cancer Sci 2022;113(8):2668–80 [eng].
[39] Costăchescu B, Niculescu A-G, Dabija MG, Teleanu RI, Grumezescu AM, Eva L. Novel strategies for spinal cord regeneration. Int J Mol Sci 2022;23(9) [eng].
[40] Martinez B, Peplow PV. MicroRNAs in blood and cerebrospinal fluid as diagnostic biomarkers of multiple sclerosis and to monitor disease progression. Neural Regen Res 2020;15(4):606–19 [eng].
[41] van Niel G, D'Angelo G, Raposo G. Shedding light on the cell biology of extracellular vesicles. Nat Rev Mol Cell Biol 2018;19(4):213–28 [eng].
[42] Butti R, Das S, Gunasekaran VP, Yadav AS, Kumar D, Kundu GC. Receptor tyrosine kinases (RTKs) in breast cancer: signaling, therapeutic implications and challenges. Mol Cancer 2018;17(1):34 [eng].
[43] He Y, Sun MM, Zhang GG, Yang J, Chen KS, Xu WW, et al. Targeting PI3K/Akt signal transduction for cancer therapy. Signal Transduct Targeted Ther 2021;6(1):425 [eng].
[44] Chen J, Zhang X, Liu X, Zhang C, Shang W, Xue J, et al. Ginsenoside Rg1 promotes cerebral angiogenesis via the PI3K/Akt/mTOR signaling pathway in ischemic mice. Eur J Pharmacol 2019;856:172418 [eng].
[45] Fei Y, Zhao B, Zhu J, Fang W, Li Y. XQ-1H promotes cerebral angiogenesis via activating PI3K/Akt/GSK3β/β-catenin/VEGF signal in mice exposed to cerebral ischemic injury. Life Sci 2021;272:119234 [eng].
[46] Yu Q, Liao M, Sun C, Zhang Q, Deng W, Cao X, et al. LBO-EMSC hydrogel serves a dual function in spinal cord injury restoration the PI3K-Akt-mTOR pathway. ACS Appl Mater Interfaces 2021;13(41):48365–77 [eng].
[47] Xu S, Wang J, Zhong J, Shao M, Jiang J, Song J, et al. CD73 alleviates GSDMD-mediated microglia pyroptosis in spinal cord injury through PI3K/AKT/Foxo1 signaling. Clin Transl Med 2021;11(1):e269 [eng].
[48] Huang J-H, He H, Chen Y-N, Liu Z, Romani MD, Xu Z-Y, et al. Exosomes derived from M2 macrophages improve angiogenesis and functional recovery after spinal cord injury through HIF-1α/VEGF Axis. Brain Sci 2022;12(10) [eng].